# Yrast structure of the shell model nucleus $^{89}$Nb

Purnima Singh,* R. Palit, S. Saha, J. Sethi, S. Biswas, and D. Choudhury
*Department of Nuclear and Atomic Physics, Tata Institute of Fundamental Research, Mumbai-400005, India*

P. C. Srivastava
*Department of Physics, Indian Institute of Technology, Roorkee-247667, India*

T. Trivedi
*Guru Ghasidas Vishwavidyalaya, Bilaspur-495009, India*

(Received 17 April 2014; revised manuscript received 6 June 2014; published 11 July 2014)

Yrast and near-yrast states in odd-$A$ $^{89}$Nb were investigated using the $^{65}$Cu($^{28}$Si,$2p2n$) reaction at a beam energy of 105 MeV. The $\gamma$-ray coincidence events were recorded with the Indian National Gamma Array spectrometer. About 30 new transitions have been observed extending the level structure of this nucleus up to spin $45/2\hbar$ and excitation energy of 10.5 MeV. Large-scale shell model calculations were performed using the effective interactions JUN45 and jj44b to understand the structure of the observed states. Reasonable agreement between the experimental observation and shell model calculations suggests that no cross-shell excitations are important up to the maximum spin observed in the current experiment.

DOI: 10.1103/PhysRevC.90.014306 PACS number(s): 21.10.−k, 23.20.Lv, 23.20.En, 27.50.+e

## I. INTRODUCTION

The level structures of nuclei in the $Z \sim 40$, $N \sim 50$ region can be well described by the shell model, thereby offering an ideal platform to test its predictions. With respect to an inert $^{56}$Ni core, the valence space in these nuclei comprise the major shell $Z,N = 28 - 50$, i.e., the orbitals $f_{5/2}$, $p_{3/2}$, $p_{1/2}$, and $g_{9/2}$. Considering $^{88}_{38}$Sr$_{50}$ as the core and restricting the valence nucleons to occupy the $p_{1/2}$ and $g_{9/2}$ subshells only, the results of shell model calculations have been observed to be in reasonable agreement with experiment for the low-spin excitations [1–5]. However, for explaining the high-spin states, a larger configuration space should be involved and even the excitation across the $N = 50$ shell closure has to be taken into account [6–8]. Therefore, systematic study of high-spin states in nuclei near the $N \sim 50$, $Z \sim 40$ region may provide important information on the core excitation mechanism.

In the present work, we report the results of an in-beam study of high-spin states in the $N = 48$ isotone, $^{89}$Nb ($Z = 41$), using the Indian National Gamma Array (INGA) spectrometer. The previously known level scheme in this nucleus was extended up to 10.5-MeV excitation energy and spin $45/2\hbar$. Shell model calculations have been performed to interpret the level structure of this nucleus.

In Sec. II, the experimental setup and the off-line data analysis techniques are briefly outlined. The experimental results and $^{89}$Nb level scheme are presented in Sec. III. The experimental results are interpreted in the framework of the spherical shell model in Sec. IV. Finally, a summary of the present work is given in Sec. V.

## II. EXPERIMENTAL DETAILS AND DATA ANALYSIS

High-spin states in $^{89}$Nb were investigated using the heavy-ion fusion evaporation reaction $^{65}$Cu($^{28}$Si, 2p2n)$^{89}$Nb. The 14UD TIFR-BARC Pelletron accelerator at Tata Institute of Fundamental Research (TIFR) provided the 105-MeV $^{28}$Si beam. The target consisted of a 1.0-mg/cm$^2$ thick foil of isotopically enriched $^{65}$Cu rolled with a $^{197}$Au foil of thickness 6.5 mg/cm$^2$. The $\gamma$-ray coincidence events were measured with the INGA spectrometer consisting of 15 Compton-suppressed clover detectors [9]. In a beam time of 5 days, a total of $3\times10^9$ events, with a clover detector coincidence fold $\geqslant 2$ were collected in a fast digital data acquisition (DDAQ) system based on Pixie-16 modules of XIA LLC [10]. The $\gamma$-ray energies and efficiencies were calibrated with standard $^{152}$Eu and $^{133}$Ba radioactive sources. For the offline analysis, the coincidence events were sorted into $\gamma^2$ matrices and $\gamma^3$ cubes. The software package RADWARE [11] was used for the data analysis.

The transition multipolarities were inferred from the measured angular distribution ratios $R_\theta$ [12]. To determine the $R_\theta$ ratios, the data were sorted into two asymmetric matrices. The first matrix contained events detected at angle 157° on the $x$ axis and all events (all) on the $y$ axis. The second matrix contained events detected at 90° on the $x$ axis and all events on the $y$ axis. Coincidence spectra were then constructed by setting identical gates on the $y$ axis in both the matrices. The ratio $R_\theta = \frac{I(\gamma_2^{157},\gamma_1^{\rm all})}{I(\gamma_2^{90},\gamma_1^{\rm all})}$ was observed to be 0.7 and 1.4 for pure stretched dipole and quadrupole transitions, respectively. These values were estimated from the transitions of known multipolarity in $^{86}$Zr [13], which was one of the dominant channels in the present experiment. For the nonstretched ($\Delta I = 0$) dipole transitions the value of $R_\theta$ was observed to be around 1.8. Intermediate values of $R_\theta$ between these values indicate their quadrupole-dipole

*purnima.phy@gmail.com

 

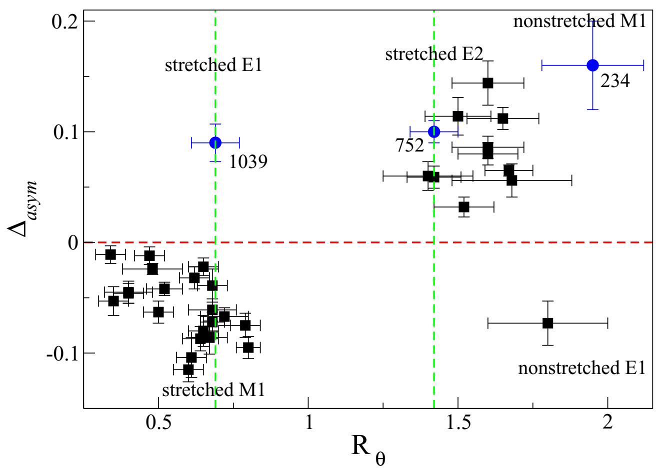


FIG. 1. (Color online) Experimental $\gamma$-ray asymmetry parameter ($\Delta_{\text{asym}}$) plotted against the angular distribution ratio ($R_\theta$) for transitions belonging to $^{89}$Nb (closed square). The dashed lines parallel to the *y* axis correspond to the values obtained for known pure stretched dipole and quadrupole transitions in $^{86}$Zr (closed circle) [13], which are labeled by their energy values in keV

mixed nature, and $R_\theta < 0.7$ was obtained for transitions with negative multipole mixing. Since, for $\Delta I = 0$ dipole transitions, the $R_\theta$ ratio is approximately the same as for a stretched quadrupole transition, a simultaneous measurement of the linear polarization can be helpful in resolving the ambiguities in the multipolarity assignment of these transitions [14,15].

To further support the multipolarity assignment, $\gamma$-ray linear polarization was extracted by considering the four crystals within a single clover detector as Compton polarimeters, where individual crystals act as scatterer, and the two adjacent crystals as observer [16,17]. For coincidence polarization measurements, the integrated polarization-directional correlation from the oriented nuclei (IPDCO) procedure was used [17]. Two asymmetric matrices were constructed from the coincidence events corresponding to single hits in any detector on one axis against clover double-hit scattered events of the 90° detector on the second axis. The scattered events were defined as either perpendicular to the reaction plane (first matrix) or parallel to the reaction plane (second matrix). The number of perpendicular $N_\perp$ and parallel $N_\parallel$ scatters for a given $\gamma$ ray were obtained by projecting out spectra gated by specific $^{89}$Nb transitions on the single-hit axis of the respective matrix. The experimental polarization asymmetry parameter was calculated as

$$\Delta_{\text{asym}} = \frac{a(E_\gamma)N_\perp - N_\parallel}{a(E_\gamma)N_\perp + N_\parallel},$$

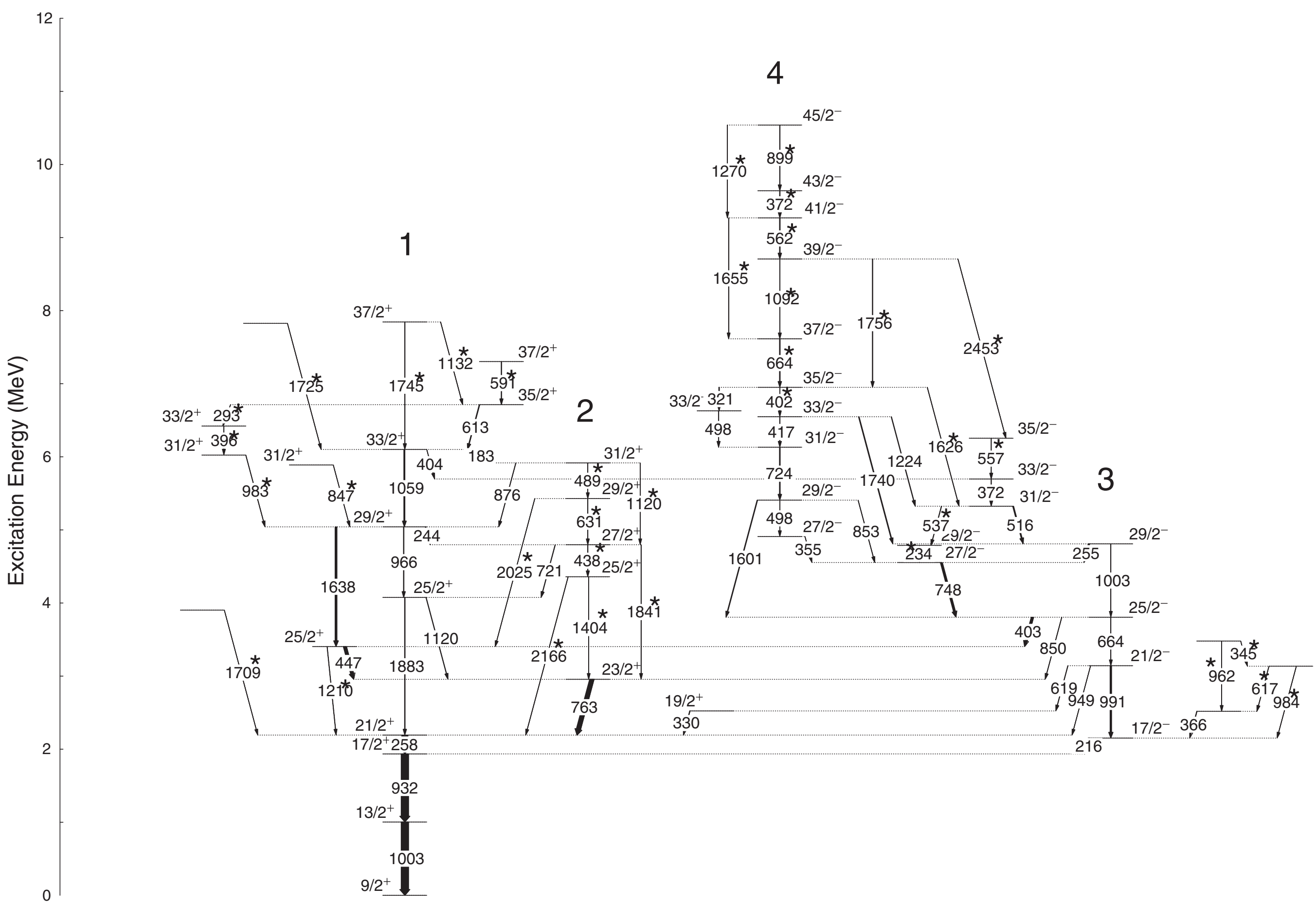


FIG. 2. Partial level scheme of $^{89}$Nb. The transitions newly identified in the present work are marked with asterisks.

TABLE I. Energies, intensities, intensity ratios, polarization asymmetry, adopted multipolarities, level energies, and spin assignments of $\gamma$-ray transitions of $^{89}$Nb.

| Energy $E_\gamma$[a] (keV) | Intensity $I_\gamma$[b] | Intensity ratio $R_\theta$ | Polarization asymmetry $\Delta_{asym}$ | Multipolarity assignment | Level energy $E_i$ (keV) | Spin assignment $J_i^\pi \rightarrow J_f^\pi$ |
|---|---|---|---|---|---|---|
| 1003.3[c] | | 1.60(10) | 0.080(10) | $E2$ | 1003.3 | $13/2^+ \rightarrow 9/2^+$ |
| 931.9 | 1000 | 1.67(8) | 0.065(5) | $E2$ | 1935.2 | $17/2^+ \rightarrow 13/2^+$ |
| 216.2 | 204(12) | 1.80(20) | −0.073(20) | $E1$ | 2151.4 | $17/2^- \rightarrow 17/2^+$ |
| 257.7 | 823(38) | 1.68(20) | 0.056(15) | $E2$ | 2192.9 | $21/2^+ \rightarrow 17/2^+$ |
| 366.4 | 42(4) | | | | 2517.8 | $\rightarrow 17/2^-$ |
| 330.1 | 56(7) | 0.68(8) | −0.061(10) | $M1$ | 2523.0 | $19/2^+ \rightarrow 21/2^+$ |
| 762.8 | 595(32) | 0.65(5) | −0.022(8) | $M1$ | 2955.7 | $23/2^+ \rightarrow 21/2^+$ |
| 617.4 | 25(5) | | | | 3135.2 | |
| 983.8 | 14(3) | | | | 3135.2 | |
| 619.0 | 39(4) | | | $E1$ | 3141.9 | $21/2^- \rightarrow 19/2^+$ |
| 949.0 | | | | $E1$ | 3141.9 | $21/2^- \rightarrow 21/2^+$ |
| 990.6 | 210(11) | 1.65(12) | 0.112(10) | $E2$ | 3141.9 | $21/2^- \rightarrow 17/2^-$ |
| 447.4 | 430(20) | 0.68(5) | -0.039(15) | $M1$ | 3403.1 | $25/2^+ \rightarrow 23/2^+$ |
| 1210.2 | 29(4) | 1.30(13) | | $E2$ | 3403.1 | $25/2^+ \rightarrow 21/2^+$ |
| 962.0 | 12 (3) | | | | 3479.8 | |
| 344.6 | | | | | 3479.8 | |
| 402.6 | 325(15) | | | $E1$ | 3805.7 | $25/2^- \rightarrow 25/2^+$ |
| 663.7[c] | | 1.40(15) | 0.060(13) | $E2$ | 3805.7 | $25/2^- \rightarrow 21/2^-$ |
| 850.0 | 28(4) | | | $E1$ | 3805.7 | $25/2^- \rightarrow 23/2^+$ |
| 1709.3 | 12(3) | | | | 3902.2 | $\rightarrow 21/2^+$ |
| 1120.1 | 43(4) | 0.69(10) | | $M1$ | 4075.8 | $25/2^+ \rightarrow 23/2^+$ |
| 1882.9 | 70(5) | 1.30(7) | | $E2$ | 4075.8 | $25/2^+ \rightarrow 21/2^+$ |
| 1403.7 | 11(2) | | | $M1$ | 4359.4 | $25/2^+ \rightarrow 23/2^+$ |
| 2166.5 | 22(5) | | | $E2$ | 4359.4 | $25/2^+ \rightarrow 21/2^+$ |
| 748.0 | 285(16) | 0.48(8) | −0.024(5) | $M1$ | 4553.7 | $27/2^- \rightarrow 25/2^-$ |
| 234.1 | 27(3) | 0.47(5) | −0.012(8) | $M1$ | 4787.8 | $29/2^- \rightarrow 27/2^-$ |
| 437.7 | 36(4) | 0.60(8) | −0.002(10) | $M1$ | 4797.1 | $27/2^+ \rightarrow 25/2^+$ |
| 721.3 | 44(6) | 0.40(8) | | $M1$ | 4797.1 | $27/2^+ \rightarrow 25/2^+$ |
| 1841.4 | 15(2) | 1.45(15) | | $E2$ | 4797.1 | $27/2^+ \rightarrow 23/2^+$ |
| 255.1 | 185(11) | | | $M1$ | 4808.8 | $29/2^- \rightarrow 27/2^-$ |
| 1003.1[c] | | | | $E2$ | 4808.8 | $29/2^- \rightarrow 25/2^-$ |
| 354.9 | 15(2) | | | $M1$ | 4908.6 | $27/2^- \rightarrow 27/2^-$ |
| 244.3 | 58(4) | 0.73(5) | | $M1$ | 5041.4 | $29/2^+ \rightarrow 27/2^+$ |
| 965.6 | 61(5) | 1.50(11) | 0.114(17) | $E2$ | 5041.4 | $29/2^+ \rightarrow 25/2^+$ |
| 1638.3 | 258(20) | 1.52(10) | 0.032(9) | $E2$ | 5041.4 | $29/2^+ \rightarrow 25/2^+$ |
| 515.7 | 139(9) | 0.52(6) | −0.042(6) | $M1$ | 5324.5 | $31/2^- \rightarrow 29/2^-$ |
| 536.7 | 42(4) | 0.72(8) | −0.067(8) | $M1$ | 5324.5 | $31/2^- \rightarrow 29/2^-$ |
| 498.5[c] | | | | $M1$ | 5407.1 | $29/2^- \rightarrow 27/2^-$ |
| 853.4 | 26(3) | | | $M1$ | 5407.1 | $29/2^- \rightarrow 27/2^-$ |
| 1601.4 | 69(5) | 1.60(12) | 0.086(10) | $E2$ | 5407.1 | $29/2^- \rightarrow 25/2^-$ |
| 631.4 | 21(3) | 0.58(6) | | $M1$ | 5428.5 | $29/2^+ \rightarrow 27/2^+$ |
| 2025.4 | 10(2) | | | $E2$ | 5428.5 | $29/2^+ \rightarrow 25/2^+$ |
| 372.1 | 58(7) | 0.67(6) | −0.086(15) | $M1$ | 5696.6 | $33/2^- \rightarrow 31/2^-$ |
| 846.6 | 14(3) | | | | 5888.0 | $\rightarrow 29/2^+$ |
| 488.7 | 14(3) | 0.47(8) | | $M1$ | 5917.2 | $31/2^+ \rightarrow 29/2^+$ |
| 875.8 | 32(4) | 0.40(5) | −0.046(9) | $M1$ | 5917.2 | $31/2^+ \rightarrow 29/2^+$ |
| 1120.1[c] | | | | $E2$ | 5917.2 | $31/2^+ \rightarrow 27/2^+$ |
| 982.9 | 28(4) | 0.34(4) | −0.011(8) | $M1$ | 6024.3 | $31/2^+ \rightarrow 29/2^+$ |
| 183.1 | 45(5) | 0.80(10) | | $M1$ | 6100.3 | $33/2^+ \rightarrow 31/2^+$ |
| 403.7 | | | | $E1$ | 6100.3 | $33/2^+ \rightarrow 33/2^-$ |
| 1058.9 | 147(8) | 1.42(9) | 0.059(10) | $E2$ | 6100.3 | $33/2^+ \rightarrow 29/2^+$ |
| 724.4 | 100(5) | 0.50(5) | −0.063(9) | $M1$ | 6131.5 | $31/2^- \rightarrow 29/2^-$ |
| 557.4 | 37(4) | 0.62(5) | −0.032(10) | $M1$ | 6254.0 | $35/2^- \rightarrow 33/2^-$ |
| 396.3 | 23(5) | 0.64(6) | −0.087(11) | $M1$ | 6420.6 | $33/2^+ \rightarrow 31/2^+$ |
| 416.9 | 46(4) | 0.60(5) | −0.115(11) | $M1$ | 6548.4 | $33/2^- \rightarrow 31/2^-$ |
| 1223.9 | 53(6) | | | $M1$ | 6548.4 | $33/2^- \rightarrow 31/2^-$ |

TABLE I. (*Continued.*)

| Energy $E_\gamma$ [a] (keV) | Intensity $I_\gamma$ [b] | Intensity ratio $R_\theta$ | Polarization asymmetry $\Delta_{asym}$ | Multipolarity assignment | Level energy $E_i$ (keV) | Spin assignment $J_i^\pi \rightarrow J_f^\pi$ |
|---|---|---|---|---|---|---|
| 1739.6 | 94(10) | 1.31(9) | 0.030(8) | $E2$ | 6548.4 | $33/2^- \rightarrow 29/2^-$ |
| 498.2 | 78(4) | 0.65(5) | −0.080(14) | $M1$ | 6629.7 | $33/2^- \rightarrow 31/2^-$ |
| 292.6 | 19(3) | 0.80(4) | −0.095(10) | $M1$ | 6713.2 | $35/2^+ \rightarrow 33/2^+$ |
| 612.9 | 86(6) | 0.68(4) | −0.072(9) | $M1$ | 6713.2 | $35/2^+ \rightarrow 33/2^+$ |
| 402.5 [c] | | | | $M1$ | 6950.9 | $35/2^- \rightarrow 33/2^-$ |
| 321.2 | 66(5) | 0.70(10) | −0.150(23) | $M1$ | 6950.9 | $35/2^- \rightarrow 33/2^-$ |
| 1626.4 | 26(4) | 1.30(8) | 0.140(32) | $E2$ | 6950.9 | $35/2^- \rightarrow 31/2^-$ |
| 590.7 | 59(3) | 0.79(5) | −0.075(11) | $M1$ | 7303.9 | $37/2^+ \rightarrow 35/2^+$ |
| 663.7 | 90(4) | 0.47(5) | | $M1$ | 7614.6 | $37/2^- \rightarrow 35/2^-$ |
| 1725.4 | 21(5) | | | | 7825.7 | $\rightarrow 33/2^+$ |
| 1131.7 | 20(4) | 0.47(9) | | $M1$ | 7844.9 | $37/2^+ \rightarrow 35/2^+$ |
| 1744.6 | 44(4) | 1.60(12) | 0.147(20) | $E2$ | 7844.9 | $37/2^+ \rightarrow 33/2^+$ |
| 1092.2 | 25(3) | 0.40(8) | −0.045(10) | $M1$ | 8706.8 | $39/2^- \rightarrow 37/2^-$ |
| 1755.9 | 58(7) | | | $E2$ | 8706.8 | $39/2^- \rightarrow 35/2^-$ |
| 2452.8 | 17(2) | | | $E2$ | 8706.8 | $39/2^- \rightarrow 35/2^-$ |
| 562.5 | 85(5) | 0.51(10) | −0.015(5) | $M1$ | 9269.3 | $41/2^- \rightarrow 39/2^-$ |
| 1654.7 | | | | $E2$ | 9269.3 | $41/2^- \rightarrow 37/2^-$ |
| 371.7 | 65(6) | 0.61(5) | −0.104(18) | $M1$ | 9641.0 | $43/2^- \rightarrow 41/2^-$ |
| 898.5 | 49(5) | 0.35(5) | −0.053(13) | $M1$ | 10539.5 | $45/2^- \rightarrow 43/2^-$ |
| 1270.2 | | | | $E2$ | 10539.5 | $45/2^- \rightarrow 41/2^-$ |

[a]The uncertainties lie between 0.5 and 1.0 keV, depending on intensity.
[b]Intensities are normalized to the 931.9 keV transition, with $I_\gamma = 1000$.
[c]Measurement of intensity and intensity ratio not possible because of the presence of $\gamma$ rays of overlapping energy.

where $a(E_\gamma)$ is a scaling factor, which corresponds to the ratio of the horizontal versus vertical coincidence count rates measured for an unpolarized source. It is a function of $\gamma$-ray energy and was determined to be 1.00(1) from the decay measurements of $^{152}$Eu and $^{133}$Ba radioactive sources. A positive polarization asymmetry value implies electric (stretched $E1$, $E2$) or nonstretched $M1$ nature for the transition, while a negative one characterizes magnetic (stretched $M1$, $M2$) or nonstretched $E1$ transitions. A near-zero value is indicative of a strong admixture. The validity of the method was verified from the known transitions in $^{89}$Nb [5] and $^{86}$Zr [13]. Figure 1 illustrates a two-dimensional plot of the asymmetry parameter, $\Delta_{asym}$, against the angular distribution ratio $R_\theta$. As can be seen from the plot, the polarization and $R_\theta$ measurements together give a reasonable assignment of the multipolarities of the transitions.

## III. RESULTS AND LEVEL SCHEME

The level scheme of $^{89}$Nb established from the present work is shown in Fig 2. The transitions have been placed on the basis of $\gamma$-$\gamma$ coincidence relations and the relative $\gamma$-transition intensities. Spin and parity assignments to the states have been made on the basis of the measured $R_\theta$ and $\Delta_{asym}$ values of the transitions depopulating these states. For these assignments, it was assumed that, in the heavy-ion induced fusion-evaporation reactions, near-yrast states are preferably populated and, thus, the spins generally increase with excitation energy. The $\gamma$-ray energies, intensities, angular distribution ratios, polarization asymmetry values, the adopted multipolarities, level energies, and spin assignments for all transitions observed in $^{89}$Nb are listed in Table I.

Prior to the present work, the nucleus $^{89}$Nb was studied through heavy-ion fusion evaporation reactions using small detector arrays [5,18]. The present work confirms the previous results. In addition, we have observed around 30 new $\gamma$-ray transitions, extending the level structure of this nucleus up to spin $45/2\hbar$ and excitation energy 10.5 MeV. In the following, new features of the level structure in $^{89}$Nb will be discussed.

### A. Positive-parity states

The positive parity states in $^{89}$Nb were reported up to 7272 keV in the previous work [5], however, the spin of the states could be determined only up to the $I^\pi = 33/2^+$ state at excitation energy 6100 keV. The lifetime of the $I^\pi = 21/2^+$ state was measured to be 19.9(6) ns by Kast *et al.*, using the electronic timing method [19]. A double-gated coincidence spectrum is displayed in Fig. 3, where the newly identified transitions depopulating positive parity states (structure 1 in Fig. 2) can be seen. A $\gamma$-ray transition of energy 613 keV, that was placed feeding the $I^\pi = 33/2^+$ state in the previous work, was confirmed by the present analysis. In addition, we were able to determine the multipolarity of this $\gamma$ ray through the $R_\theta$ and polarization measurements. A dipole transition of energy 1132 keV was also observed in coincidence with this transition. This placement is further confirmed by the observation of a 1745-keV transition in parallel with this cascade (see Fig. 2). Therefore, the state at 7845 keV was assigned a spin and parity of $37/2^+$. Another parallel decay path, consisting of a cascade of dipole transitions of energy 983, 396, and 293 keV

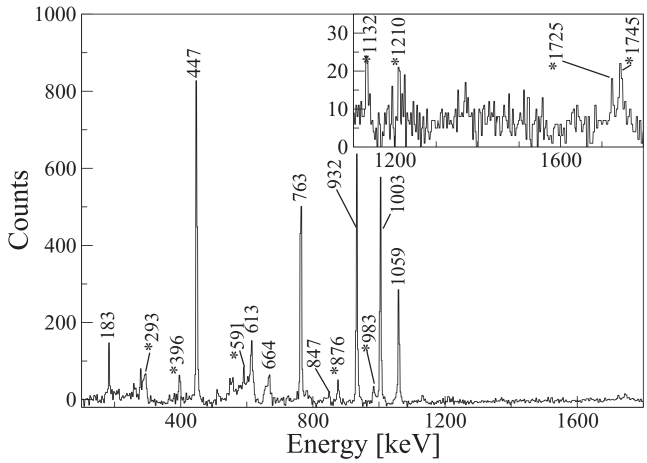


FIG. 3. Representative $\gamma$-ray coincidence spectrum showing transitions in positive parity structure 1. The spectrum was created with a double gate on 1638- and 258-keV transitions. The peaks marked with asterisks denote transitions newly identified in the present work.

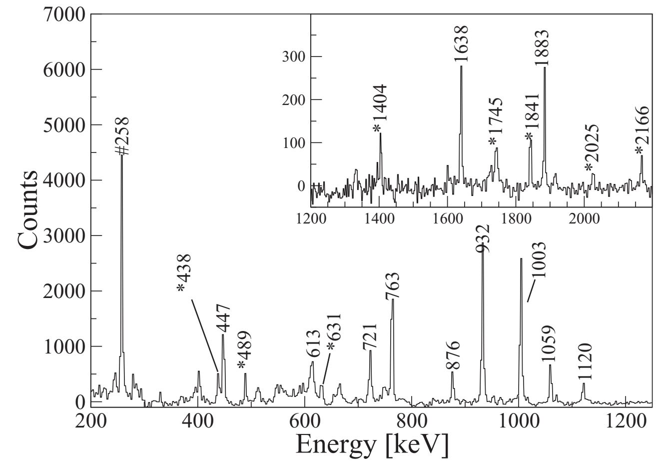


FIG. 4. Representative $\gamma$-ray coincidence spectrum showing transitions of structure 2. The spectrum was created with a gate on a list from 258-, 932-, and 1003-keV transitions, and one from a list of 1404-, 438-, 489-, 183-, and 244-keV transitions. The peaks marked with asterisks denote transitions newly identified in the present work. The hash-marked peak is an unresolved doublet.

(see Fig. 2) was observed between the states $I^\pi = 35/2^+$ and $29/2^+$. The state at $35/2^+$ is also fed by a dipole transition of energy 591 keV.

At lower spin, a gamma ray transition of energy 1709 keV was observed to feed the positive parity state at $I^\pi = 21/2^+$. We were not able to determine the multipolarity of this transition because of low statistics. Another transition of energy 1210 keV, depopulating the state at $I^\pi = 21/2^+$ was newly identified.

In the present work, we have identified a new structure labeled as 2 in Fig. 2. It consists of a cascade of four dipole gamma rays of energy 1404, 438, 631, and 489 keV. Weak $E2$ crossover transitions of energy 1841 and 1120 keV have also been identified. Figure 4 shows a double-gated coincidence spectrum, where these transitions can be easily identified. Structure 2 is connected to the previously known positive parity structure 1 through gamma rays of energy 763, 2166, 721, 2025, 387, and 876 keV. The structure was assigned positive parity through the linear polarization measurement of 763 and 876 keV transitions.

### B. Negative-parity states

In the previous work, the negative parity states in $^{89}$Nb were reported up to 5698 keV and a lifetime of 0.74(7) ns was determined for the yrast $17/2^-$ state at 2193 keV, using the recoil distance Doppler shift technique [5]. However, the spin and parity of the higher-lying levels could not be determined. In the present work, we were able to assign spin and parities to these levels, on the basis of $R_\theta$ and polarization measurements. The measured $R_\theta$ ratios, for the $\gamma$ rays of energy 372 and 516 keV, confirm their stretched dipole character, thereby assigning spin and parity of $33/2^-$ to the level at 5697 keV. We have also observed a parallel decay path between the $I^\pi = 31/2^-$ and $27/2^-$ levels consisting of gamma rays of energy 537 and 234 keV (see Fig. 5). A dipole transition of energy 557 keV was observed in coincidence with the 372-keV gamma ray and was placed on top of it.

A weakly populated sequence (labeled as 4 in Fig. 2), consisting of gamma-ray transitions of energy 498, 724, 417, 321, and 498 keV was reported in the previous work [5]. With the results of the present work, we could extend this structure up to an excitation energy of 10 540 keV. The $R_\theta$ and polarization measurement of the 1601-keV gamma ray confirms its stretched quadrupole character. Thus, negative parity was assigned to this cascade. The multipolarities of 498-, 724-, 417-, and 321-keV transitions have been observed to be consistent with dipole character (see Table I). Therefore,

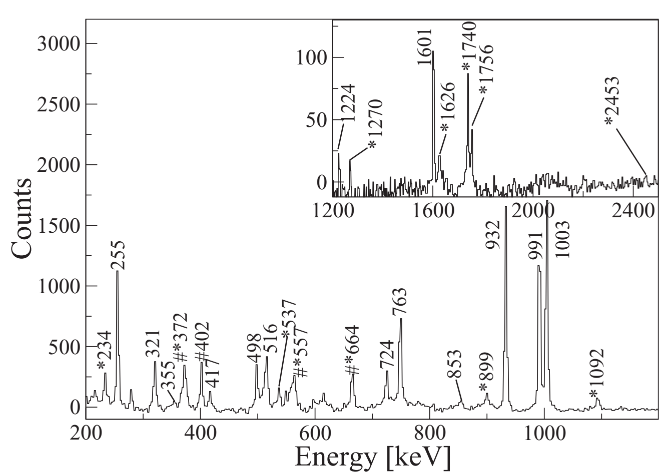


FIG. 5. Double-gated $\gamma$-ray coincidence spectrum showing transitions depopulating negative parity states (structures 3 and 4). The spectrum was created with double gate on 216- and 664-keV transitions. The peaks marked with asterisks denote transitions newly identified in the present work. Hash-marked peaks are unresolved doublets.

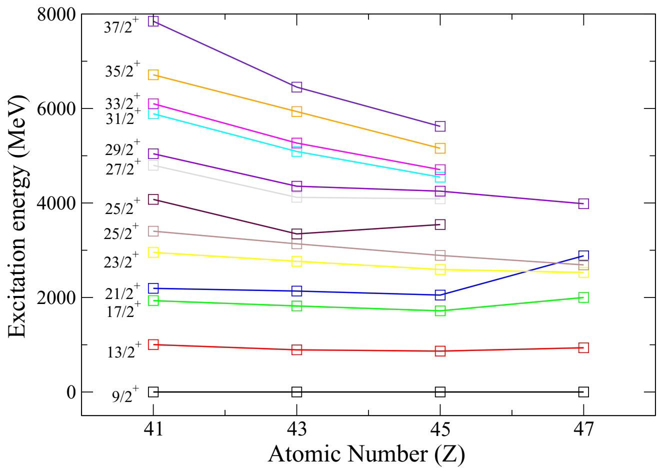


FIG. 6. (Color online) Systematics of positive parity states in odd-$A$ $N = 48$ isotones $^{89}$Nb, $^{91}$Tc [7], $^{93}$Rh [20], and $^{95}$Ag [25].

we have assigned spin and parity of $35/2^-$ to the state at 6951 keV. A cascade of gamma rays of energy 664, 1092, 562, 372, and 899 keV was observed in coincidence with the lower transitions of structure 4 (see Fig. 5) and thus have been placed in the level scheme according to their relative intensity. Their placement is further confirmed by crossover transitions of energy 1756, 1655, and 1270 keV. The measured $R_\theta$ ratio of 664-, 1092-, 562-, 372-, and 899-keV transitions are consistent with dipole character.

## IV. DISCUSSION

The low-lying yrast and near yrast excitations in $N = 48$, $Z > 38$, odd-$A$ nuclei have been successfully explained in a restricted model space consisting of $g_{9/2}$ and $p_{1/2}$ orbitals, relative to the $^{88}_{38}\mathrm{Sr}_{50}$ core [5,7,19,20]. However, to explain the high-spin states, excitations of protons from $f_{5/2}$ or $p_{3/2}$ are also to be taken into account, as evident from recent works in neighboring nuclei with $Z \sim 38$, $N \sim 48$ [6,21–24].

The energies of the positive parity states in $N = 48$, odd-$A$ nuclei, $^{89}$Nb, $^{91}$Tc [7], $^{93}$Rh [20], and $^{95}$Ag [25] are plotted in Fig. 6. Irrespective of their $Z$, the level spacings in the spectrum for all the nuclei are observed to be similar up to the $I = 25/2^+$ state. This suggests that the wave functions of these states can be described in a simple seniority scheme picture, where the dominant contribution is from seniority $v = 3$ configurations involving quasiparticles in the $g_{9/2}$ orbitals. In contrast, the second excited $25/2^+$ state shows irregular behavior suggesting a large mixing of states with seniority 3 and 5. At higher angular momentum, the effect of the proton-neutron ($T = 0$) interaction on the one, two, and three extra proton pairs in $^{91}$Tc, $^{93}$Rh, and $^{95}$Ag, respectively, causes a deviation from this simple seniority scheme [26]. As a result a systematic compression of the $v = 5$ states is observed with increase in $Z$.

To understand the configuration of the observed states in $^{89}$Nb, shell model calculations have been performed, using the shell model code ANTOINE [27]. The valence space employed in the calculations, comprise the major shell $Z,N = 28$–50, with an inert $^{56}$Ni core. The valence particles have been allowed to move freely between the $f_{5/2}$, $p_{3/2}$, $p_{1/2}$, and $g_{9/2}$ orbitals. Two recently derived effective interactions, JUN45 [28] and jj44b [29] have been used in the calculations. The JUN45 interaction is a realistic interaction based on the Bonn-C potential, derived by fitting 400 experimental binding and excitation energy data out of 69 nuclei in the $A = 63 \sim 96$ mass region [28]. While fitting JUN45 interaction, the experimental data were not taken from $N = Z$ nuclei, specifically the Ni and Cu isotopes because the considered model space is not sufficient to describe collectivity for these nuclei, which is significantly from excitation of the $f_{7/2}$ nucleons. The JUN45 interaction is successful along the $N \sim 50$ isotone chains, whereas close to the Ni region, the results are not satisfactory, because of the exclusion of the effects of $\pi f_{7/2}$ excitations. The jj44b interaction from Brown and Lisetskiy [29] is also a realistic interaction based on Bonn-C potential. It was developed by fitting 600 binding energies and excitation energies from nuclei with $Z = 28 - 30$ and $N = 48 - 50$. The jj44b interaction was reported to give considerably better agreement in nuclei near $Z = 28$ [30,31], because it incorporates the influence of $f_{7/2}$ excitations. Shell model calculations using both these effective interactions were observed to give good agreement with the experimental data in the neighboring nuclei $^{88,89}$Zr [22,23]. The single-particle energies used with the JUN45 interaction are –9.8280 ($p_{3/2}$), –8.7087 ($f_{5/2}$), –7.8388 ($p_{1/2}$), and –6.2617 ($g_{9/2}$) MeV. For the jj44b interaction, the single-particle energies are –9.6566 ($p_{3/2}$), –9.2859 ($f_{5/2}$), –8.2695 ($p_{1/2}$), and –5.8944 ($g_{9/2}$) MeV.

A comparison of the experimental excitation energies of the positive and negative parity states of $^{89}$Nb with the predictions of shell model calculations is shown in Figs. 7 and 8, respectively. The experimental data cover the range of spins observed in the current work as well as the $1/2^-$ state taken from the literature [32]. The dominant wave functions for these states are shown in Table II.

The ground state, $I^\pi = 9/2^+$, is nicely reproduced by the jj44b interaction, whereas, the JUN45 interaction predicts an $I^\pi = 1/2^-$ ground state, and the $I^\pi = 9/2^+$ state at an excitation energy of 67 keV. The dominant contribution for the $I^\pi = 9/2^+$ state, as predicted by JUN45 is of $\pi(g^1_{9/2})$ configuration, contrary to the jj44b configuration, which predicts a dominant $\pi(g^3_{9/2})$ contribution. For the low-lying states, up to spin $25/2^+$, the configuration $[\pi(p^4_{3/2}f^6_{5/2}p^2_{1/2}g^1_{9/2}) \otimes \nu(p^4_{3/2}f^6_{5/2}p^2_{1/2}g^8_{9/2}]$ is predicted to play a dominant role. The two nonyrast $I^\pi = 25/2^+$ states observed in experiment have dominant contributions from seniority 5 states involving proton excitations from the $p_{1/2}$ to the $g_{9/2}$ orbital. All the states from $I^\pi = 27/2^+$ to $37/2^+$ are well described by seniority 5 configurations involving proton excitations from the $p_{1/2}$ to the $g_{9/2}$ orbital. However, the third excited $I^\pi = 31/2^+$ and second excited $I^\pi = 37/2^+$ states involve excitation from the $f_{5/2}$ to the $g_{9/2}$ orbital. For higher lying states with spin up to $37/2^+$, the results of the JUN45 interaction are close to the experiment, whereas, those of jj44b are roughly 500–750 keV higher.

To further check the reliability of the two interactions, the reduced transition probability for the $21/2^+ \longrightarrow 17/2^+$ decay

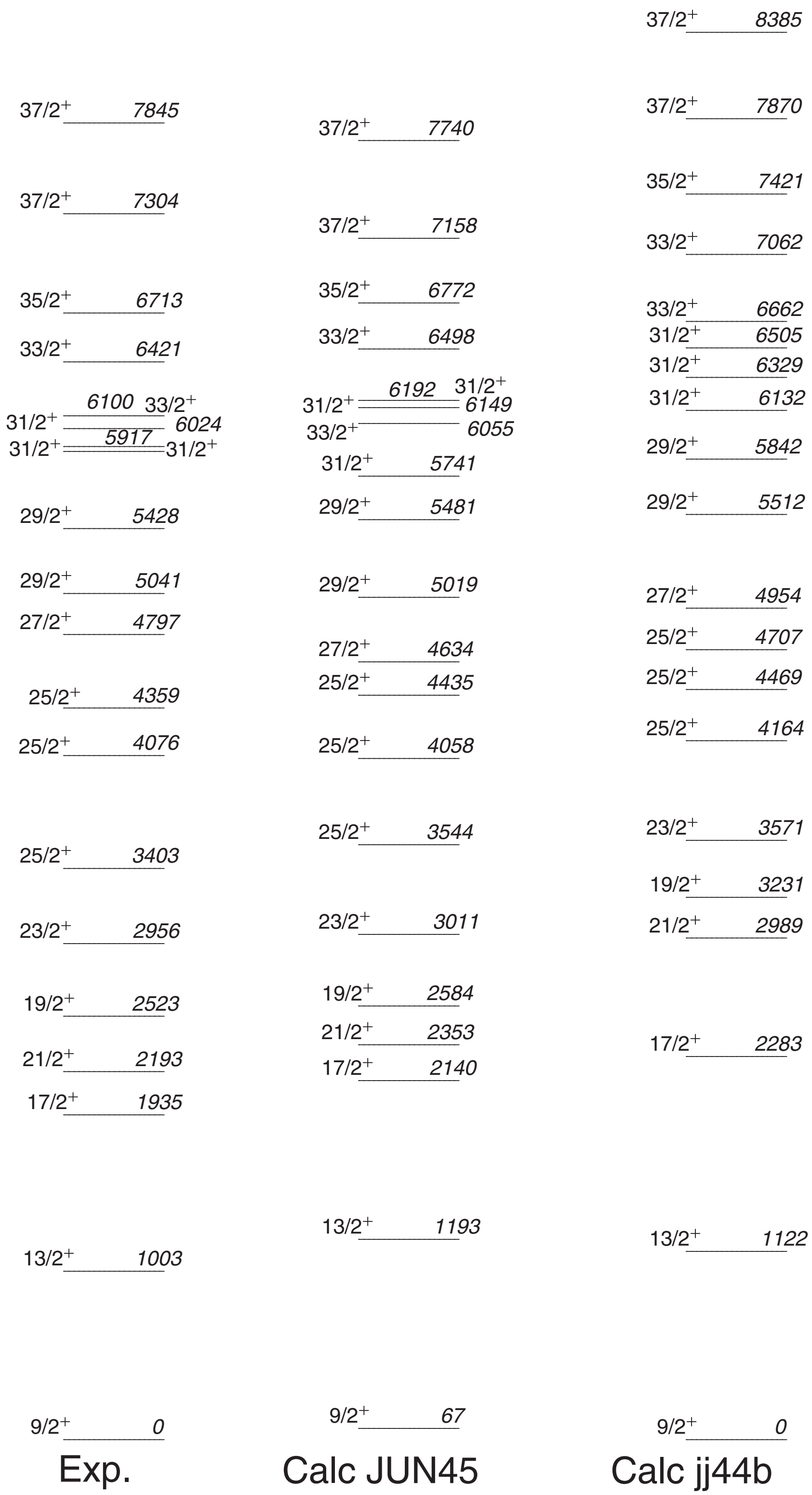


FIG. 7. Experimental and calculated positive parity states in $^{89}$Nb .

was calculated using an effective charge of $e_p = 1.5e$ and $e_n = 0.5e$ for proton and neutron, respectively. The JUN45 interaction predicts a B($E2$, $21/2^+ \longrightarrow 17/2^+$) value of 1.00 W.u, whereas the same predicted using jj44b is 2.21 W.u. Although both the values are in reasonable agreement with the reported value of 1.46(5) W.u [19], the difference between the excitation energies of the $21/2^+$ and $17/2^+$ levels predicted by the jj44b interaction is 706 keV, which is quite large. On the other hand, the predicted difference using the JUN45 interaction is 213 keV, which is very close to the observed value of 258 keV.

The calculated negative parity states have been compared to the observed states in Fig. 8. As discussed in the previous section, the JUN45 interaction predicts the $I^\pi = 1/2^-$ state

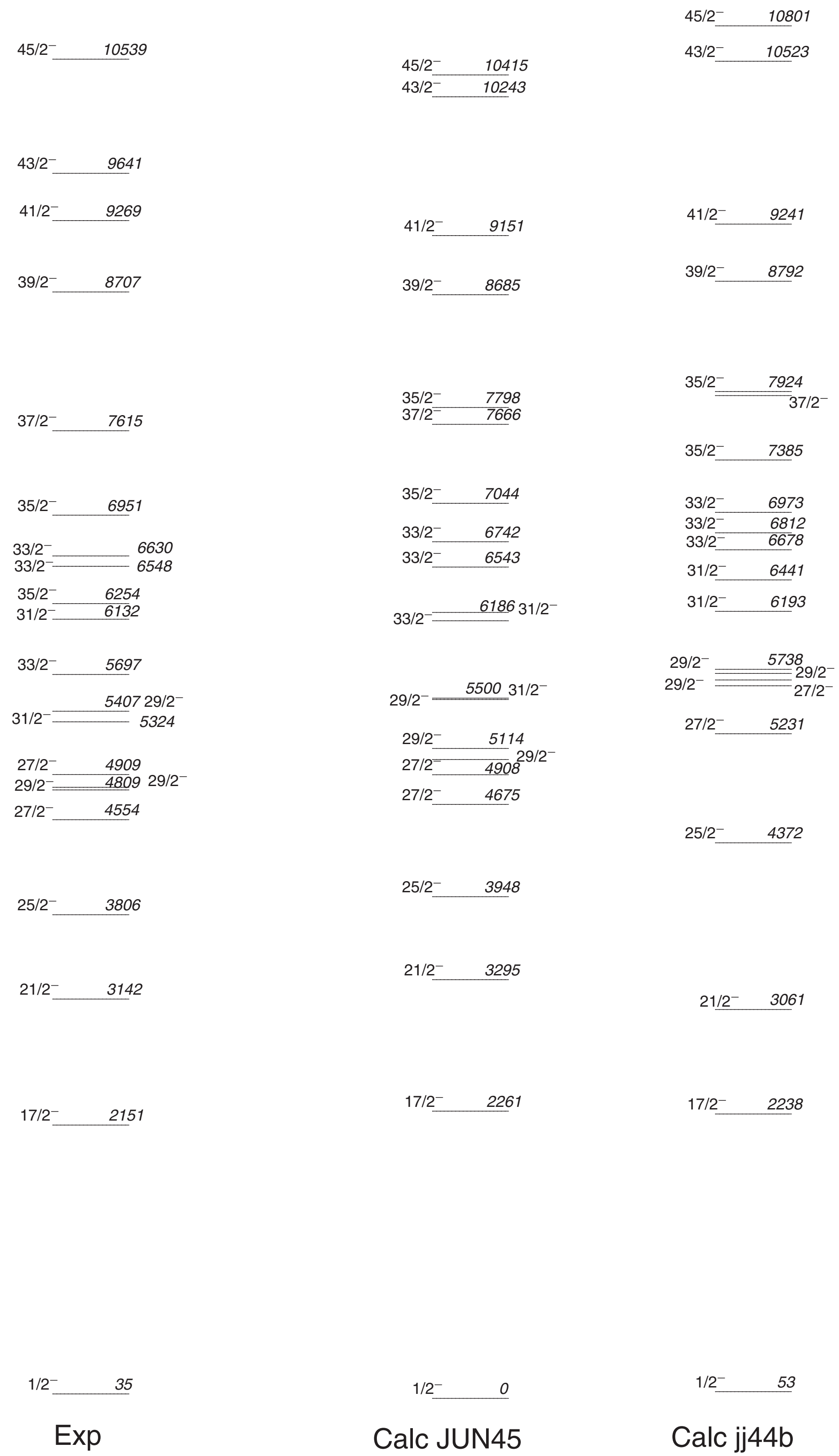


FIG. 8. Experimental and calculated negative parity states in $^{89}$Nb. The experimental data for $I^{\pi} = 1/2^{-}$ state was taken from Ref. [32].

TABLE II. Main partitions of wave functions of the positive and negative parity states in $^{89}$Nb.

| | | JUN45 Wave functions | | | jj44b Wave functions | |
|---|---|---|---|---|---|---|
| $I$ | Probability | Proton | Neutron | Probability | Proton | Neutron |
| $9/2^+_{\mathrm{g.s.}}$ | 21.8 % | $p_{3/2}^{4}f_{5/2}^{6}p_{1/2}^{2}g_{9/2}^{1}$ | $p_{3/2}^{4}f_{5/2}^{6}p_{1/2}^{2}g_{9/2}^{8}$ | 11.2 % | $p_{3/2}^{4}f_{5/2}^{6}p_{1/2}^{0}g_{9/2}^{3}$ | $p_{3/2}^{4}f_{5/2}^{6}p_{1/2}^{2}g_{9/2}^{8}$ |
| $13/2^+_1$ | 22.3 % | $p_{3/2}^{4}f_{5/2}^{6}p_{1/2}^{0}g_{9/2}^{3}$ | $p_{3/2}^{4}f_{5/2}^{6}p_{1/2}^{2}g_{9/2}^{8}$ | 12.6 % | $p_{3/2}^{4}f_{5/2}^{6}p_{1/2}^{0}g_{9/2}^{3}$ | $p_{3/2}^{4}f_{5/2}^{6}p_{1/2}^{2}g_{9/2}^{8}$ |
| $17/2^+_1$ | 32.3% | $p_{3/2}^{4}f_{5/2}^{6}p_{1/2}^{2}g_{9/2}^{1}$ | $p_{3/2}^{4}f_{5/2}^{6}p_{1/2}^{2}g_{9/2}^{8}$ | 14.6 % | $p_{3/2}^{4}f_{5/2}^{6}p_{1/2}^{0}g_{9/2}^{3}$ | $p_{3/2}^{4}f_{5/2}^{6}p_{1/2}^{2}g_{9/2}^{8}$ |
| $21/2^+_1$ | 41.7 % | $p_{3/2}^{4}f_{5/2}^{6}p_{1/2}^{2}g_{9/2}^{1}$ | $p_{3/2}^{4}f_{5/2}^{6}p_{1/2}^{2}g_{9/2}^{8}$ | 16.0% | $p_{3/2}^{4}f_{5/2}^{6}p_{1/2}^{2}g_{9/2}^{1}$ | $p_{3/2}^{4}f_{5/2}^{6}p_{1/2}^{2}g_{9/2}^{8}$ |
| $19/1^+_1$ | 45.1 % | $p_{3/2}^{4}f_{5/2}^{6}p_{1/2}^{2}g_{9/2}^{1}$ | $p_{3/2}^{4}f_{5/2}^{6}p_{1/2}^{2}g_{9/2}^{8}$ | 16.4 % | $p_{3/2}^{4}f_{5/2}^{6}p_{1/2}^{2}g_{9/2}^{1}$ | $p_{3/2}^{4}f_{5/2}^{6}p_{1/2}^{2}g_{9/2}^{8}$ |
| $23/2^+_1$ | 37.7% | $p_{3/2}^{4}f_{5/2}^{6}p_{1/2}^{2}g_{9/2}^{1}$ | $p_{3/2}^{4}f_{5/2}^{6}p_{1/2}^{2}g_{9/2}^{8}$ | 19.2 % | $p_{3/2}^{4}f_{5/2}^{6}p_{1/2}^{0}g_{9/2}^{3}$ | $p_{3/2}^{4}f_{5/2}^{6}p_{1/2}^{2}g_{9/2}^{8}$ |
| $25/2^+_1$ | 35.3 % | $p_{3/2}^{4}f_{5/2}^{6}p_{1/2}^{2}g_{9/2}^{1}$ | $p_{3/2}^{4}f_{5/2}^{6}p_{1/2}^{2}g_{9/2}^{8}$ | 21.0 % | $p_{3/2}^{4}f_{5/2}^{6}p_{1/2}^{0}g_{9/2}^{3}$ | $p_{3/2}^{4}f_{5/2}^{6}p_{1/2}^{2}g_{9/2}^{8}$ |
| $25/2^+_2$ | 34.9 % | $p_{3/2}^{4}f_{5/2}^{6}p_{1/2}^{0}g_{9/2}^{3}$ | $p_{3/2}^{4}f_{5/2}^{6}p_{1/2}^{2}g_{9/2}^{8}$ | 18.0 % | $p_{3/2}^{4}f_{5/2}^{6}p_{1/2}^{0}g_{9/2}^{3}$ | $p_{3/2}^{4}f_{5/2}^{6}p_{1/2}^{2}g_{9/2}^{8}$ |
| $25/2^+_3$ | 29.8 % | $p_{3/2}^{4}f_{5/2}^{6}p_{1/2}^{0}g_{9/2}^{3}$ | $p_{3/2}^{4}f_{5/2}^{6}p_{1/2}^{2}g_{9/2}^{8}$ | 18.9 % | $p_{3/2}^{4}f_{5/2}^{5}p_{1/2}^{1}g_{9/2}^{3}$ | $p_{3/2}^{4}f_{5/2}^{6}p_{1/2}^{2}g_{9/2}^{8}$ |
| $27/2^+_1$ | 38.7 % | $p_{3/2}^{4}f_{5/2}^{6}p_{1/2}^{0}g_{9/2}^{3}$ | $p_{3/2}^{4}f_{5/2}^{6}p_{1/2}^{2}g_{9/2}^{8}$ | 22.1 % | $p_{3/2}^{4}f_{5/2}^{5}p_{1/2}^{0}g_{9/2}^{4}$ | $p_{3/2}^{4}f_{5/2}^{5}p_{1/2}^{2}g_{9/2}^{9}$ |
| $29/2^+_1$ | 40.5 % | $p_{3/2}^{4}f_{5/2}^{6}p_{1/2}^{0}g_{9/2}^{3}$ | $p_{3/2}^{4}f_{5/2}^{6}p_{1/2}^{2}g_{9/2}^{8}$ | 23.3 % | $p_{3/2}^{4}f_{5/2}^{6}p_{1/2}^{0}g_{9/2}^{3}$ | $p_{3/2}^{4}f_{5/2}^{6}p_{1/2}^{2}g_{9/2}^{8}$ |
| $29/2^+_2$ | 40.2 % | $p_{3/2}^{4}f_{5/2}^{6}p_{1/2}^{0}g_{9/2}^{3}$ | $p_{3/2}^{4}f_{5/2}^{6}p_{1/2}^{2}g_{9/2}^{8}$ | 18.0 % | $p_{3/2}^{4}f_{5/2}^{6}p_{1/2}^{0}g_{9/2}^{3}$ | $p_{3/2}^{4}f_{5/2}^{6}p_{1/2}^{2}g_{9/2}^{8}$ |
| $31/2^+_1$ | 44.2 % | $p_{3/2}^{4}f_{5/2}^{6}p_{1/2}^{0}g_{9/2}^{3}$ | $p_{3/2}^{4}f_{5/2}^{6}p_{1/2}^{2}g_{9/2}^{8}$ | 30.9 % | $p_{3/2}^{4}f_{5/2}^{5}p_{1/2}^{0}g_{9/2}^{4}$ | $p_{3/2}^{4}f_{5/2}^{5}p_{1/2}^{2}g_{9/2}^{9}$ |
| $33/2^+_1$ | 48.4 % | $p_{3/2}^{4}f_{5/2}^{6}p_{1/2}^{0}g_{9/2}^{3}$ | $p_{3/2}^{4}f_{5/2}^{6}p_{1/2}^{2}g_{9/2}^{8}$ | 29.4% | $p_{3/2}^{4}f_{5/2}^{6}p_{1/2}^{0}g_{9/2}^{3}$ | $p_{3/2}^{4}f_{5/2}^{6}p_{1/2}^{2}g_{9/2}^{8}$ |
| $31/2^+_2$ | 37.2 % | $p_{3/2}^{4}f_{5/2}^{6}p_{1/2}^{0}g_{9/2}^{3}$ | $p_{3/2}^{4}f_{5/2}^{6}p_{1/2}^{2}g_{9/2}^{8}$ | 26.2 % | $p_{3/2}^{4}f_{5/2}^{6}p_{1/2}^{0}g_{9/2}^{3}$ | $p_{3/2}^{4}f_{5/2}^{6}p_{1/2}^{2}g_{9/2}^{8}$ |
| $31/2^+_3$ | 32.2 % | $p_{3/2}^{4}f_{5/2}^{5}p_{1/2}^{1}g_{9/2}^{3}$ | $p_{3/2}^{4}f_{5/2}^{6}p_{1/2}^{2}g_{9/2}^{8}$ | 35.1% | $p_{3/2}^{4}f_{5/2}^{5}p_{1/2}^{1}g_{9/2}^{3}$ | $p_{3/2}^{4}f_{5/2}^{6}p_{1/2}^{2}g_{9/2}^{8}$ |
| $33/2^+_2$ | 45.8 % | $p_{3/2}^{4}f_{5/2}^{6}p_{1/2}^{0}g_{9/2}^{3}$ | $p_{3/2}^{4}f_{5/2}^{6}p_{1/2}^{2}g_{9/2}^{8}$ | 23.6 % | $p_{3/2}^{4}f_{5/2}^{5}p_{1/2}^{1}g_{9/2}^{3}$ | $p_{3/2}^{4}f_{5/2}^{6}p_{1/2}^{2}g_{9/2}^{8}$ |
| $35/2^+_1$ | 50.5 % | $p_{3/2}^{4}f_{5/2}^{6}p_{1/2}^{0}g_{9/2}^{3}$ | $p_{3/2}^{4}f_{5/2}^{6}p_{1/2}^{2}g_{9/2}^{8}$ | 30.8 % | $p_{3/2}^{4}f_{5/2}^{6}p_{1/2}^{0}g_{9/2}^{3}$ | $p_{3/2}^{4}f_{5/2}^{6}p_{1/2}^{2}g_{9/2}^{8}$ |
| $37/2^+_1$ | 50.5 % | $p_{3/2}^{4}f_{5/2}^{6}p_{1/2}^{0}g_{9/2}^{3}$ | $p_{3/2}^{4}f_{5/2}^{6}p_{1/2}^{2}g_{9/2}^{8}$ | 30.1 % | $p_{3/2}^{4}f_{5/2}^{6}p_{1/2}^{0}g_{9/2}^{3}$ | $p_{3/2}^{4}f_{5/2}^{6}p_{1/2}^{2}g_{9/2}^{8}$ |
| $37/2^+_2$ | 49.4 % | $p_{3/2}^{4}f_{5/2}^{5}p_{1/2}^{1}g_{9/2}^{3}$ | $p_{3/2}^{4}f_{5/2}^{6}p_{1/2}^{2}g_{9/2}^{8}$ | 51.8% | $p_{3/2}^{4}f_{5/2}^{5}p_{1/2}^{1}g_{9/2}^{3}$ | $p_{3/2}^{4}f_{5/2}^{6}p_{1/2}^{2}g_{9/2}^{8}$ |
| $1/2^-_1$ | 44.4 % | $p_{3/2}^{4}f_{5/2}^{6}p_{1/2}^{1}g_{9/2}^{2}$ | $p_{3/2}^{4}f_{5/2}^{6}p_{1/2}^{2}g_{9/2}^{8}$ | 19.6 % | $p_{3/2}^{4}f_{5/2}^{6}p_{1/2}^{1}g_{9/2}^{2}$ | $p_{3/2}^{4}f_{5/2}^{6}p_{1/2}^{2}g_{9/2}^{8}$ |
| $17/2^-_1$ | 51.3 % | $p_{3/2}^{4}f_{5/2}^{6}p_{1/2}^{1}g_{9/2}^{2}$ | $p_{3/2}^{4}f_{5/2}^{6}p_{1/2}^{2}g_{9/2}^{8}$ | 9.3 % | $p_{3/2}^{4}f_{5/2}^{6}p_{1/2}^{1}g_{9/2}^{2}$ | $p_{3/2}^{4}f_{5/2}^{6}p_{1/2}^{2}g_{9/2}^{8}$ |
| $21/2^-_1$ | 58.2 % | $p_{3/2}^{4}f_{5/2}^{6}p_{1/2}^{1}g_{9/2}^{2}$ | $p_{3/2}^{4}f_{5/2}^{6}p_{1/2}^{2}g_{9/2}^{8}$ | 15.1 % | $p_{3/2}^{4}f_{5/2}^{6}p_{1/2}^{0}g_{9/2}^{3}$ | $p_{3/2}^{4}f_{5/2}^{5}p_{1/2}^{2}g_{9/2}^{9}$ |
| $21/2^-_2$ | 52.5 % | $p_{3/2}^{4}f_{5/2}^{6}p_{1/2}^{1}g_{9/2}^{2}$ | $p_{3/2}^{4}f_{5/2}^{6}p_{1/2}^{2}g_{9/2}^{8}$ | 14.7 % | $p_{3/2}^{4}f_{5/2}^{6}p_{1/2}^{1}g_{9/2}^{2}$ | $p_{3/2}^{4}f_{5/2}^{6}p_{1/2}^{2}g_{9/2}^{8}$ |
| $21/2^-_3$ | 19.4 % | $p_{3/2}^{4}f_{5/2}^{6}p_{1/2}^{0}g_{9/2}^{3}$ | $p_{3/2}^{4}f_{5/2}^{5}p_{1/2}^{2}g_{9/2}^{9}$ | 12.2 % | $p_{3/2}^{4}f_{5/2}^{6}p_{1/2}^{1}g_{9/2}^{2}$ | $p_{3/2}^{4}f_{5/2}^{6}p_{1/2}^{2}g_{9/2}^{8}$ |
| $23/2^-_1$ | 48.7 % | $p_{3/2}^{4}f_{5/2}^{6}p_{1/2}^{1}g_{9/2}^{2}$ | $p_{3/2}^{4}f_{5/2}^{6}p_{1/2}^{2}g_{9/2}^{8}$ | 13.6 % | $p_{3/2}^{4}f_{5/2}^{5}p_{1/2}^{1}g_{9/2}^{3}$ | $p_{3/2}^{4}f_{5/2}^{5}p_{1/2}^{2}g_{9/2}^{9}$ |
| $25/2^-_1$ | 59.8 % | $p_{3/2}^{4}f_{5/2}^{6}p_{1/2}^{1}g_{9/2}^{2}$ | $p_{3/2}^{4}f_{5/2}^{6}p_{1/2}^{2}g_{9/2}^{8}$ | 15.0 % | $p_{3/2}^{4}f_{5/2}^{5}p_{1/2}^{1}g_{9/2}^{3}$ | $p_{3/2}^{4}f_{5/2}^{5}p_{1/2}^{2}g_{9/2}^{9}$ |
| $27/2^-_1$ | 63.8 % | $p_{3/2}^{4}f_{5/2}^{6}p_{1/2}^{1}g_{9/2}^{2}$ | $p_{3/2}^{4}f_{5/2}^{6}p_{1/2}^{2}g_{9/2}^{8}$ | 19.9% | $p_{3/2}^{4}f_{5/2}^{5}p_{1/2}^{1}g_{9/2}^{3}$ | $p_{3/2}^{4}f_{5/2}^{5}p_{1/2}^{2}g_{9/2}^{9}$ |
| $27/2^-_2$ | 55.3% | $p_{3/2}^{4}f_{5/2}^{6}p_{1/2}^{1}g_{9/2}^{2}$ | $p_{3/2}^{4}f_{5/2}^{6}p_{1/2}^{2}g_{9/2}^{8}$ | 29.6% | $p_{3/2}^{4}f_{5/2}^{6}p_{1/2}^{1}g_{9/2}^{2}$ | $p_{3/2}^{4}f_{5/2}^{6}p_{1/2}^{2}g_{9/2}^{8}$ |
| $29/2^-_1$ | 63.8 % | $p_{3/2}^{4}f_{5/2}^{6}p_{1/2}^{1}g_{9/2}^{2}$ | $p_{3/2}^{4}f_{5/2}^{6}p_{1/2}^{2}g_{9/2}^{8}$ | 25.3 % | $p_{3/2}^{4}f_{5/2}^{5}p_{1/2}^{0}g_{9/2}^{4}$ | $p_{3/2}^{4}f_{5/2}^{6}p_{1/2}^{2}g_{9/2}^{8}$ |
| $29/2^-_2$ | 66.0 % | $p_{3/2}^{4}f_{5/2}^{6}p_{1/2}^{1}g_{9/2}^{2}$ | $p_{3/2}^{4}f_{5/2}^{6}p_{1/2}^{2}g_{9/2}^{8}$ | 17.4 % | $p_{3/2}^{4}f_{5/2}^{5}p_{1/2}^{1}g_{9/2}^{3}$ | $p_{3/2}^{4}f_{5/2}^{5}p_{1/2}^{2}g_{9/2}^{9}$ |
| $29/2^-_3$ | 47.8% | $p_{3/2}^{4}f_{5/2}^{6}p_{1/2}^{1}g_{9/2}^{2}$ | $p_{3/2}^{4}f_{5/2}^{6}p_{1/2}^{2}g_{9/2}^{8}$ | 10.7 % | $p_{3/2}^{4}f_{5/2}^{4}p_{1/2}^{1}g_{9/2}^{4}$ | $p_{3/2}^{4}f_{5/2}^{6}p_{1/2}^{2}g_{9/2}^{8}$ |
| $31/2^-_1$ | 65.8 % | $p_{3/2}^{4}f_{5/2}^{6}p_{1/2}^{1}g_{9/2}^{2}$ | $p_{3/2}^{4}f_{5/2}^{6}p_{1/2}^{2}g_{9/2}^{8}$ | 46.9 % | $p_{3/2}^{4}f_{5/2}^{6}p_{1/2}^{1}g_{9/2}^{2}$ | $p_{3/2}^{4}f_{5/2}^{6}p_{1/2}^{2}g_{9/2}^{8}$ |
| $33/2^-_1$ | 63.7 % | $p_{3/2}^{4}f_{5/2}^{6}p_{1/2}^{1}g_{9/2}^{2}$ | $p_{3/2}^{4}f_{5/2}^{6}p_{1/2}^{2}g_{9/2}^{8}$ | 43.3 % | $p_{3/2}^{4}f_{5/2}^{5}p_{1/2}^{0}g_{9/2}^{4}$ | $p_{3/2}^{4}f_{5/2}^{6}p_{1/2}^{2}g_{9/2}^{8}$ |
| $31/2^-_2$ | 54.9 % | $p_{3/2}^{4}f_{5/2}^{6}p_{1/2}^{1}g_{9/2}^{2}$ | $p_{3/2}^{4}f_{5/2}^{6}p_{1/2}^{2}g_{9/2}^{8}$ | 32.3 % | $p_{3/2}^{4}f_{5/2}^{5}p_{1/2}^{0}g_{9/2}^{4}$ | $p_{3/2}^{4}f_{5/2}^{6}p_{1/2}^{2}g_{9/2}^{8}$ |
| $31/2^-_3$ | 47.0 % | $p_{3/2}^{4}f_{5/2}^{5}p_{1/2}^{2}g_{9/2}^{2}$ | $p_{3/2}^{4}f_{5/2}^{6}p_{1/2}^{2}g_{9/2}^{8}$ | 14.6 % | $p_{3/2}^{4}f_{5/2}^{5}p_{1/2}^{1}g_{9/2}^{3}$ | $p_{3/2}^{4}f_{5/2}^{5}p_{1/2}^{2}g_{9/2}^{9}$ |
| $33/2^-_1$ | 40.2 % | $p_{3/2}^{4}f_{5/2}^{5}p_{1/2}^{2}g_{9/2}^{2}$ | $p_{3/2}^{4}f_{5/2}^{6}p_{1/2}^{2}g_{9/2}^{8}$ | 48.6 % | $p_{3/2}^{4}f_{5/2}^{6}p_{1/2}^{1}g_{9/2}^{2}$ | $p_{3/2}^{4}f_{5/2}^{6}p_{1/2}^{2}g_{9/2}^{8}$ |
| $33/2^-_2$ | 45.1 % | $p_{3/2}^{4}f_{5/2}^{5}p_{1/2}^{2}g_{9/2}^{2}$ | $p_{3/2}^{4}f_{5/2}^{6}p_{1/2}^{2}g_{9/2}^{8}$ | 30.0 % | $p_{3/2}^{4}f_{5/2}^{5}p_{1/2}^{0}g_{9/2}^{4}$ | $p_{3/2}^{4}f_{5/2}^{6}p_{1/2}^{2}g_{9/2}^{8}$ |
| $35/2^-_1$ | 41.4 % | $p_{3/2}^{4}f_{5/2}^{5}p_{1/2}^{2}g_{9/2}^{2}$ | $p_{3/2}^{4}f_{5/2}^{6}p_{1/2}^{2}g_{9/2}^{8}$ | 39.9 % | $p_{3/2}^{4}f_{5/2}^{5}p_{1/2}^{0}g_{9/2}^{4}$ | $p_{3/2}^{4}f_{5/2}^{6}p_{1/2}^{2}g_{9/2}^{8}$ |
| $37/2^-_1$ | 34.6 % | $p_{3/2}^{4}f_{5/2}^{5}p_{1/2}^{0}g_{9/2}^{4}$ | $p_{3/2}^{4}f_{5/2}^{6}p_{1/2}^{2}g_{9/2}^{8}$ | 44.4 % | $p_{3/2}^{4}f_{5/2}^{5}p_{1/2}^{0}g_{9/2}^{4}$ | $p_{3/2}^{4}f_{5/2}^{6}p_{1/2}^{2}g_{9/2}^{8}$ |
| $35/2^-_2$ | 33.9 % | $p_{3/2}^{4}f_{5/2}^{5}p_{1/2}^{0}g_{9/2}^{4}$ | $p_{3/2}^{4}f_{5/2}^{6}p_{1/2}^{2}g_{9/2}^{8}$ | 24.1% | $p_{3/2}^{4}f_{5/2}^{5}p_{1/2}^{2}g_{9/2}^{2}$ | $p_{3/2}^{4}f_{5/2}^{6}p_{1/2}^{2}g_{9/2}^{8}$ |
| $37/2^-_2$ | 57.1 % | $p_{3/2}^{4}f_{5/2}^{5}p_{1/2}^{0}g_{9/2}^{4}$ | $p_{3/2}^{4}f_{5/2}^{6}p_{1/2}^{2}g_{9/2}^{8}$ | 42.5 % | $p_{3/2}^{4}f_{5/2}^{5}p_{1/2}^{0}g_{9/2}^{4}$ | $p_{3/2}^{4}f_{5/2}^{6}p_{1/2}^{2}g_{9/2}^{8}$ |
| $39/2^-_1$ | 66.7 % | $p_{3/2}^{4}f_{5/2}^{5}p_{1/2}^{0}g_{9/2}^{4}$ | $p_{3/2}^{4}f_{5/2}^{6}p_{1/2}^{2}g_{9/2}^{8}$ | 52.2 % | $p_{3/2}^{4}f_{5/2}^{5}p_{1/2}^{0}g_{9/2}^{4}$ | $p_{3/2}^{4}f_{5/2}^{6}p_{1/2}^{2}g_{9/2}^{8}$ |
| $41/2^-_1$ | 67.2 % | $p_{3/2}^{4}f_{5/2}^{5}p_{1/2}^{0}g_{9/2}^{4}$ | $p_{3/2}^{4}f_{5/2}^{6}p_{1/2}^{2}g_{9/2}^{8}$ | 49.2 % | $p_{3/2}^{4}f_{5/2}^{5}p_{1/2}^{0}g_{9/2}^{4}$ | $p_{3/2}^{4}f_{5/2}^{6}p_{1/2}^{2}g_{9/2}^{8}$ |
| $43/2^-_1$ | 67.9 % | $p_{3/2}^{4}f_{5/2}^{5}p_{1/2}^{0}g_{9/2}^{4}$ | $p_{3/2}^{4}f_{5/2}^{6}p_{1/2}^{2}g_{9/2}^{8}$ | 50.8 % | $p_{3/2}^{4}f_{5/2}^{5}p_{1/2}^{0}g_{9/2}^{4}$ | $p_{3/2}^{4}f_{5/2}^{6}p_{1/2}^{2}g_{9/2}^{8}$ |
| $45/2^-_1$ | 69.3 % | $p_{3/2}^{4}f_{5/2}^{5}p_{1/2}^{0}g_{9/2}^{4}$ | $p_{3/2}^{4}f_{5/2}^{6}p_{1/2}^{2}g_{9/2}^{8}$ | 56.0 % | $p_{3/2}^{4}f_{5/2}^{5}p_{1/2}^{0}g_{9/2}^{4}$ | $p_{3/2}^{4}f_{5/2}^{6}p_{1/2}^{2}g_{9/2}^{8}$ |

to be the ground state, whereas in experiment this state is observed at an excitation energy of 35 keV [32]. The predicted excitation energy of 53 keV, for the $I^\pi = 1/2^-$ state, using jj44b, shows better agreement with experiment. The lowest negative parity state observed in the present experiment is at spin $17/2^-$ with excitation energy 2151 keV. The difference between calculated and observed excitation energies for this state is 109 and 87 keV for JUN45 and jj44b interactions, respectively. This state has a dominant contribution from the $[\pi(p_{3/2}^4 f_{5/2}^6 p_{1/2}^1 g_{9/2}^2) \otimes \nu(p_{3/2}^4 f_{5/2}^6 p_{1/2}^2 g_{9/2}^8)]$ configuration. The same configuration continues to dominate up to spin $31/2^-$. Up to the $I^\pi = 27/2^-$ state, the experimental results show a remarkable agreement with the results of the shell model calculations using the JUN45 interaction, the agreement being within 150 keV, however, the ordering of the second excited $I^\pi = 27/2^-$ state and $I^\pi = 29/2^-$ states is not reproduced by the calculations. From $I^\pi = 31/2^-$ to $35/2^-$, the states are predicted to have dominant contribution of proton excitation from the $f_{5/2}$ to the $p_{1/2}$ orbital. However, this configuration does not give a satisfying explanation for the observed experimental trends. For example, the energy difference between the $I^\pi = 33/2^-$ state becomes as large as 422 keV and the lowest $I^\pi = 35/2^-$ state observed experimentally is also not reproduced in the calculations. The second excited $I^\pi = 35/2^-$ state and states above $I^\pi = 37/2^-$ involve excitation of protons from the $f_{5/2}$ and $p_{1/2}$ orbitals to the $g_{9/2}$ orbital. The states calculated using jj44b show large deviation from experiment between the $I^\pi = 25/2^-$ and $35/2^-$ states, which increases with spin, becoming as large as 1131 keV for the $I^\pi = 35/2^-$ state. From $I^\pi = 37/2^-$ to $45/2^-$ states, the calculation matches well with experiment for both the interactions, except for the $43/2^-$ state, which is predicted to be 602 keV and 882 keV higher in JUN45 and jj44b interactions, respectively.

In general, except for the inversion of two closely spaced states, the $9/2^+$ and $1/2^-$ levels, the results of the shell model calculations using the JUN45 interaction have been observed to be in better agreement with the experimental excitation energies up to the highest spin observed. The experimentally observed highest spin states with $I^\pi = 37/2^+$ and $45/2^-$ are reproduced in the calculation within a 200-keV difference. On the other hand, the calculations using the jj44b interaction reproduce the correct ordering of the $I^\pi = 9/2^+$ and $I^\pi = 1/2^-$ state, however, at high spin, the calculated states are predicted around 800–1000 keV higher than experiment.

The overall agreement of the experimental level energies, with those predicted by shell model calculations, suggests that the excitations across the $N = 50$ shell gap do not play any significant role in forming the yrast structure of this nucleus up to the highest spin observed in the current experiment. A detailed study of electromagnetic transition probabilities can give further insight into the exact nature of wave functions of these states.

It is also somewhat surprising that, although the expected angular momentum imparted classically in the current heavy-ion fusion evaporation reaction is $\sim 60\hbar$, we were not able to observe any further excited states. Here, it is to be noted that the intensity of the transitions depopulating the observed highest spin states in the current experiment is around 5%–6% of the channel strength, which is quite large and the array was sensitive enough to enable observation of transitions with intensities $\sim 1\%$ (see Table I). No evidence of any discrete levels above $I \sim 23\hbar$ could possibly indicate a large change in structure of this nucleus at high spin, which may involve a highly fragmented decay path consisting of several weak high-energy gamma rays or even existence of a high-spin isomer, thereby making it difficult to observe further excited states. Another possibility could be that the states based on excitations across the $N = 50$ shell gap are very high in energy, probably above particle threshold, and the nucleus decays preferentially through a particle channel. Further experimental investigations are required to explore these possibilities.

## V. SUMMARY

In summary, excited states in $^{89}$Nb were populated via the $^{65}$Cu($^{28}$Si,2p2n) reaction at a beam energy of 105 MeV. The gamma-ray coincidence events were measured with the Indian National Gamma Array spectrometer consisting of 15 Compton-suppressed clover detectors. Measurements of linear polarization and angular distribution have led to the firm assignment of the spins and parities of high-spin states in this nucleus. About 30 new transitions have been observed, extending the level structure of this nucleus to a spin of $45/2\hbar$ and an excitation energy of 10.5 MeV. To understand the structure of the observed states, large-scale shell model calculations were performed using the effective interactions JUN45 and jj44b. The results of shell model calculations using the JUN45 interaction have been observed to be in better agreement with experimental excitation energies up to the highest spin observed. On the other hand the calculations with jj44b show poor agreement with the experimental observation, especially at high spin. The fair agreement of the observed states with those predicted by shell model calculations suggest that no $N = 50$ cross-shell excitations are important up to the maximum spin observed in the current experiment. A detailed study of electromagnetic transition probabilities is required to understand the exact nature of wave functions of these states.

## ACKNOWLEDGMENTS

Authors are thankful to the staff at TIFR-BARC Pelletron Linac Facility and all the members of the INGA collaboration. Support from S. V. Jadhav, R. Donthi, B. S. Naidu, and P. B. Chavan during the experiment is gratefully acknowledged. This work was partially supported by the Department of Science and Technology, Government of India under Grant No. IR/S2/PF-03/2003-II.

[1] D. H. Gloeckner and F. J. D. Serduke, Nucl. Phys. A **220**, 477 (1974).

[2] R. Gross and A. Frenkel, Phys. Lett. B **53**, 227 (1974).

[3] K. Oxorn, S. K. Mark, J. E. Kitching, and S. S. M. Wong, Z. Phys. A **321**, 485 (1985).
[4] A. Amusa and R. D. Lawson, Z. Phys. A **314**, 205 (1983).
[5] A. Bödeker, K. P. Lieb, C. J. Gross, M. K. Kabadiyski, D. Rudolph, M. Weiszflog, J. Eberth, H. Grawe, J. Heese, and K.-H. Maier, Phys. Rev. C **48**, 1617 (1993).
[6] S. E. Arnell, D. Foltescu, H. A. Roth, Ö. Skeppstedt, J. Blomqvist, A. Nilsson, T. Kuroyanagi, S. Mitarai, and J. Nyberg, Phys. Rev. C **49**, 51 (1994).
[7] D. Rudolph *et al.*, Phys. Rev. C **49**, 66 (1994).
[8] S. Ray, N. S. Pattabiraman, R. Goswami, S. S. Ghugre, A. K. Sinha, and U. Garg, Phys. Rev. C **69**, 054314 (2004).
[9] R. Palit *et al.*, Nucl. Instrum. Methods A **680**, 90 (2012).
[10] H. Tan *et al.*, in *Proceedings of the IEEE Nuclear Science Symposium and Medical Imaging Conference (2008 NSS/MIC), Dresdan* (IEEE, New York, 2009), p. 2471
[11] D. C. Radford, Nucl. Instrum. Methods A **361**, 297 (1995).
[12] M. Piiparinen *et al.*, Nucl. Phys. A **605**, 191 (1996).
[13] E. K. Warburton, C. J. Lister, J. W. Olness, P. E. Haustein, S. K. Saha, D. E. Alburger, J. A. Becker, R. A. Dewberry, and R. A. Naumann, Phys. Rev. C **31**, 1211 (1985).
[14] D. Sohler *et al.*, Phys. Rev. C **85**, 044303 (2012).
[15] Y. Zheng *et al.*, Phys. Rev. C **87**, 044328 (2013).
[16] G. Duchêne *et al.*, Nucl. Instrum. Methods Phys. Res. A **432**, 90 (1999).
[17] K. Starosta *et al.*, Nucl. Instrum. Methods Phys. Res. A **423**, 16 (1999).
[18] P. Singh, R. G. Pillay, J. A. Sheikh, and H. G. Devare, Phys. Rev. C **48**, 1609 (1993).
[19] D. Kast, K. P. Lieb, C. J. Gross, A. Jungclaus, D. Rudolph, R. Schubart, H. Grawe, and J. Heese, Nucl. Phys. A **587**, 202 (1995).
[20] H. A. Roth, S. E. Arnell, J. Blomqvist, D. Foltescu, T. Kuroyanagi, S. Mitarai, A. Nilsson, J. Nyberg, and O. Skeppstedt, J. Phys. G **21**, L1 (1995).
[21] R. Schwengner *et al.*, Phys. Rev. C **57**, 2892 (1998).
[22] S. Saha, R. Palit, J. Sethi, S. Biswas, P. Singh, T. Trivedi, D. Choudhury, and P. C. Srivastava, Phys. Rev. C **89**, 044315 (2014).
[23] S. Saha *et al.*, Phys. Rev. C **86**, 034315 (2012).
[24] C. J. Xu *et al.*, Phys. Rev. C **86**, 027302 (2012).
[25] J. Doring *et al.*, Phys. Rev. C **68**, 034306 (2003).
[26] I. Talmi, La Rivista del Nuovo Cimento **3**, 85 (1973).
[27] E. Caurier, G. Martnez-Pinedo, F. Nowacki, A. Poves, and A. P. Zuker, Rev. Mod. Phys. **77**, 427 (2005).
[28] M. Honma, T. Otsuka, T. Mizusaki, and M. Hjorth-Jensen, Phys. Rev. C **80**, 064323 (2009).
[29] B. A. Brown and A. F. Lisetskiy (unpublished); see also endnote (28) in B. Cheal *et al.*, Phys. Rev. Lett. **104**, 252502 (2010).
[30] C. J. Chiara *et al.*, Phys. Rev. C **85**, 024309 (2012).
[31] M. Albers *et al.*, Phys. Rev. C **88**, 054314 (2013).
[32] P. W. Gallagher, N. K. Aras, and W. B. Walters, Phys. Rev. C **23**, 873 (1981).